MECH. STRUCT. & MACH., 29(3), 351–371 (2001)

DESIGN SENSITIVITY ANALYSIS AND OPTIMIZATION OF NONLINEAR TRANSIENT DYNAMICS*

Nam H. Kim† and Kyung K. Choi#

Center for Computer-Aided Design and Department of Mechanical Engineering, College of Engineering, University of Iowa, Iowa City, IA 52242

ABSTRACT

A shape design sensitivity analysis (DSA) and optimization of structural transient dynamics are proposed for the finite deformation elastoplastic materials under impact with a rigid surface. A shape variation of the structure is considered using the material derivative approach in continuum mechanics. Hyperelasticity-based multiplicatively decomposed elastoplasticity is used for the constitutive model. The implicit Newmark time integration scheme is used for the structural dynamics. The design sensitivity equation is solved at each converged time step with the same tangent stiffness matrix as response analysis without iteration. The cost of sensitivity computation is more efficient than the cost of response analysis for the implicit time integration method. The efficiency and the accuracy of the proposed method are shown through the design optimization of a vehicle bumper.

*Communicated by D. Tortorelli.

†Corresponding author. E-mail: nkim@ccad.uiowa.edu

#E-mail: kkchoi@ccad.uiowa.edu

I. INTRODUCTION

When a time-dependent load and/or boundary condition is applied to a structure, the transient response of the structure is important. The inertia effect and wave propagation through the structure are important compared to the quasi-static response. Methods of integration for the equation of motion in a dynamic response analysis can be implicit or explicit. The explicit integration method is usually used with a very small time-step size to solve a wave propagation problem associated with a relatively local response of structure. This method is useful for impact and crash-worthiness problems for which wave effects such as focusing, reflection, and diffraction are important. The implicit integration method is usually used to solve inertial problems [1] for which the overall dynamic response of a structure is sought. The structural problems are considered inertial when the response time is longer than the time required for the wave to traverse the structure. Since in the linear problem the implicit integration scheme is unconditionally stable by choosing appropriate integration parameters, the time step is usually one or two orders of magnitude larger than that of the explicit integration method. However, a reasonable time-step size must be chosen based on the accuracy of the solution [2].

Recently, several research results were reported for design sensitivity analysis (DSA) of structural dynamics. For nonlinear elastic material with infinitesimal deformation assumption, Tortorelli et al. [3] formulated an adjoint sensitivity equation, and Poldneff and Arora [4] addressed design sensitivity for thermoviscoelasticity using the implicit time integration method. Pollock and Noor [5] derived the sensitivity expression of a structural dynamic problem with respect to material properties using the explicit central difference method to take the derivative of the finite-element matrix equation. For elastic material, the sensitivity expression is consistent with that of response analysis.

Arora and Dutta [6] formulated design sensitivity equations for dynamic elastoplastic problems. They claimed that the design sensitivity equation uses a different tangent stiffness matrix from that of response analysis because of finite rotational effect. To overcome this difference from response analysis, sensitivity iteration is carried out using the same tangent stiffness matrix as response analysis, which reduces the efficiency of sensitivity computation significantly.

Choi and Cho [7] discussed design sensitivity expressions for dynamic elastoplastic problems using the explicit central difference method for the beam element. The sensitivity expression for the explicit time integration method is simpler than that for the implicit method. The cost of sensitivity computation, however, may not be less than the response analysis time. Thus, the merit of the sensitivity computation is reduced compared to the finite difference method for explicit time integration. It is quite beneficial to develop a sensitivity equation for the implicit time integration method since it does not require iteration

for the finite deformation elastoplastic problem, so the cost of sensitivity computation is significantly less than that of the finite difference method.

Recently, Kim et al. [8] proposed an efficient way of computing design sensitivity of the finite deformation elastoplasticity based on the hyperelastic constitutive relation with multiplicative decomposition of the deformation gradient.

In this article, an efficient shape DSA of structural transient dynamics is proposed for finite deformation elastoplastic materials, including impact with the rigid surface. The direct differentiation method is used instead of the adjoint variable method. It is well known that the adjoint variable method for the transient dynamic problems with an initial condition becomes a terminal value problem for which a terminal condition is given for an adjoint equation [9]. Thus, the adjoint equation cannot be solved simultaneously with the response analysis. This fact complicates significantly calculations associated with transient dynamic DSA using the adjoint variable method.

The Newmark time integration scheme is used to integrate in the time domain for the implicit method. The computational aspect of time integration methods is compared from the sensitivity analysis viewpoint. A linear system of the design sensitivity equation is solved at each converged time step.

Hyperelasticity-based multiplicative decomposition elastoplasticity is used for the constitutive model that can represent finite deformation and rigid body rotation. The stress-strain relation is described as a hyperelastic relation between the intermediate rotation-free configuration and the current configuration. For shape DSA, however, the variation of the intermediate configuration is transformed into the undeformed domain in which the design velocity field is defined since the design perturbation is always defined at the initial undeformed geometry. Through an appropriate transformation, an updated Lagrangian form of the design sensitivity equation is obtained. The consistent tangent operator is used to obtain quadratic convergence of response analysis and accurate sensitivity results. Design sensitivity is path dependent as response analysis; the sensitivity equation is solved at each converged time. However, using the consistent tangent stiffness matrix, the sensitivity equation can be solved without iteration. After solving the design sensitivity equation, the material derivatives of other path-dependent variables are updated to be used at the next configuration time.

The efficiency and accuracy of the proposed method are shown through the design optimization of a vehicle bumper.

II. RESPONSE ANALYSIS OF STRUCTURAL DYNAMICS

Response analysis of nonlinear structural transient dynamics is reviewed in this section. The implicit time integration method is discussed with an accel-

eration formulation. Using the implicit method, the nonlinear transient response is obtained by solving for incremental acceleration with a linearization procedure. For details, refer to the work of Hughes [10] for the linear problem and the work of Bathe [11] for the nonlinear problem. For given $\boldsymbol{f}^b$, $\boldsymbol{f}^h$, and $\boldsymbol{\zeta}$, the weak form of the equation of motion for a structural dynamic problem at time $t \in [0,T]$ is to find the displacement function $z(\boldsymbol{x},\boldsymbol{u},\boldsymbol{t}) \in V$ such that

$$d(z_{,tt},\bar{z}) + a(z,\bar{z}) = \ell(\bar{\mathbf{z}}), \qquad \forall \bar{z} \in Z \tag{1}$$

where

$$V = \{z(\boldsymbol{x},t) \,|\, z(\boldsymbol{x},t) = \boldsymbol{\zeta}(\boldsymbol{x},t),\ \mathbf{x} \in \Gamma^g,\ z(\boldsymbol{x},t) \in \boldsymbol{H}^1\ (\Omega)\} \tag{2}$$

is the solution space, Z is the space of the kinematically admissible displacement, $\boldsymbol{f}^b$ is the body force, $\boldsymbol{f}^h$ is the surface traction force on the boundary Γ^h, and $\mathbf{Z}$ is the prescribed displacement vector on the boundary Γ^g. The overbar is used to denote the first-order variation in this article. If the problem contains structural impact, then the contact variational form $b(z,\bar{z})$ can be added as discussed in the work of Kim et al. [12]. The $b(z,\bar{z})$ term is ignored in the following derivation. In Eq. 1,

$$d(z_{,tt},\bar{z}) = \int_{0_\Omega} \rho \bar{z}^T z_{,tt} d\boldsymbol{\Omega} \tag{3}$$

is the kinetic energy form. In Eq. 3, $z_{,tt}$ is the second time derivative of the displacement (i.e., acceleration), and ρ is the initial density of the material. Using the conservation of mass, the integration in Eq. 3 can be carried out at the undeformed configuration with the density at that configuration. In Eq. 1,

$$a(z,\bar{z}) = \int_{0_\Omega} \sigma_{ij} \bar{\varepsilon}_{ij} d\boldsymbol{\Omega} \tag{4}$$

$$\ell(\bar{z}) = \int_{0_\Omega} \bar{z}^T \boldsymbol{f}^b \, d\boldsymbol{\Omega} + \int_{0_{\Gamma^h}} \bar{z}^T \boldsymbol{f}^h \, d\boldsymbol{\Gamma} \tag{5}$$

are the structural energy and load forms, respectively. The structural energy form depends on the constitutive model of the material. In this article, a finite deformation elastoplastic constitutive model is assumed for $a(z,\bar{z})$ with a multiplicative decomposition of the deformation gradient into elastic and plastic parts as

$$\boldsymbol{F}(\boldsymbol{X}) = \boldsymbol{F}^e(\boldsymbol{X}) \boldsymbol{F}^p(\boldsymbol{X}) \tag{6}$$

The Kirchhoff stress σ_{ij} can be obtained using hyperelasticity with $\boldsymbol{F}^e(\boldsymbol{X})$. Note that the integration domain ${}^0\Omega$ in Eq. 4 is undeformed configuration since the Kirchhoff stress is used instead of the Cauchy stress. For general elastoplastic problem, Ω_{ij} is computed by a return-mapping algorithm in the principal stress space by fixing $\boldsymbol{F}^p(\boldsymbol{X})$. The configuration determined by $\boldsymbol{F}^p(\boldsymbol{X})$ is called the *stress-free intermediate configuration*. For the load form, only the conservative load case is considered for simplicity; this is independent of the displace-

ment. Note that the structural energy form is generally nonlinear, whereas kinetic energy and load forms are linear. Since Eq. 1 is an initial boundary value problem (IBVP), the following initial conditions are used:

$$z(\boldsymbol{X},0) = z^0(\boldsymbol{X}) \qquad \boldsymbol{X} \in {}^0\boldsymbol{\Omega} \tag{7}$$

$$z_{,t}(\boldsymbol{X},0) = z^0_{,t}(\boldsymbol{X}) \qquad \boldsymbol{X} \in {}^0\boldsymbol{\Omega} \tag{8}$$

where $z^0(\boldsymbol{x})$ and $z^0_{,t}(\boldsymbol{x})$ are the prescribed initial displacement and velocity vectors, respectively. For solving the IBVP Eq. 1 numerically, the finite difference method is used to make the time domain discrete, whereas the mesh-free method is used for the structural domain. The discretization of the structural domain using the mesh-free method was discussed in detail by Chen et al. [13]. Time discretization is derived in the following.

To solve the differential Eq. 1 with initial conditions Eqs. 7 and 8, the time interval $[0,T]$ is discretized by $[t_1, t_2, \ldots, t_n, \ldots, t_N]$, and the equilibrium Eq. 1 is imposed at each discrete time. Let the equation of motion in Eq. 1 be satisfied at time t_{n-1}, and the solution at time t_n is investigated. The Newmark family time integration with the predictor-corrector method is used to integrate Eq. 1 as

$${}^n z_{,t} = {}^n z^{pr}_{,t} + \gamma \Delta t^n \, {}^n z_{,tt} \tag{9}$$

$${}^n z = {}^n z^{pr} + \beta \Delta t^2 \, {}^n z_{,tt} \tag{10}$$

where

$${}^n z^{pr}_{,t} = {}^{n-1} z_{,t} + (1 - \gamma)\Delta t \, {}^{n-1} z_{,tt} \tag{11}$$

$${}^n z^{pr} = {}^{n-1} z + \Delta t \, {}^{n-1} z_{,t} + (\tfrac{1}{2} - \beta)\Delta t^2 \, {}^{n-1} z_{,tt} \tag{12}$$

are the velocity and displacement predictors, respectively, and are constructed based on the configuration at the previous time t_{n-1}. The left superscripts n and $n-1$ denote the configuration times t_n and t_{n-1}, respectively. Here, β and γ are integration parameters for the Newmark method, and Δt is the time-step size. Since the right sides of Eqs. 9 and 10 include responses at time t_n, this integration method is implicit; thus, iteration is usually required.

The stability and accuracy of the time integration method for the linear system were discussed rigorously by Hughes [10]. The unconditionally stable condition for the Newmark family integration method is given by $2\beta \geq \gamma \geq 1/2$ and the second-order accuracy is preserved only when $\gamma = 1/2$, which does not include any viscous damping effects. The other choice of $\gamma > 1/2$ yields the first-order accuracy with viscous damping effects.

Since the structural energy form in Eq. 4 is nonlinear, a linearization is required to solve the nonlinear equation iteratively using the Newton-Raphson method. The linearization of the structural variational form was discussed thor-

oughly by Simo [14]. The linearized form of $a(z,\bar{z})$ is denoted by $a^*(z;\Delta z,\bar{z})$, which is linear with respect to Δz and $\bar{z}$, and depends on the configuration at t_n, as

$$a^*(z;\Delta z,\bar{z}) \equiv \int_{0_\Omega} (\bar{\varepsilon}_{ij} c_{ijkl} \varepsilon_{kl}(\Delta z) + \sigma_{ij} \eta_{ij}(\Delta z,\bar{z})) d\Omega \tag{13}$$

where c_{ijkl} is the fourth-order consistent tangent tensor [14], ε_{ij} is the engineering strain tensor with respect to the current configuration, and η_{ij} is the geometric strain tensor term. Equation 13 is the updated Lagrangian formulation [11] since the current configuration is used as the reference. Let the current configuration time be t_n and the right superscript $k+1$ denote the current iteration counter. The linearized incremental equation of motion becomes

$$d(\Delta z^{k+1}_{,tt},\bar{z}) + a^*({}^n z^k;\Delta z^{k+1},\bar{z}) = \ell(\bar{z}) - a({}^n z^k,\bar{z}) - d({}^n z^k_{,tt},\bar{z}), \qquad \forall \bar{z} \in Z \tag{14}$$

Since only the relation between the incremental displacement and incremental acceleration is required in Eq. 14, the following incremental integration formulations of the displacement are used:

$$\Delta z^{k+1} = \beta \Delta t^2 \Delta z^{k+1}_{,tt} \tag{15}$$

$${}^n z^{k+1} = {}^n z^k + \Delta z^{k+1} \tag{16}$$

where ${}^n z^0 = {}^n z^{pr}$ is the predictor at the time t_n. Note that since the kinetic energy form is linear, it does not require a linearization. Equation 14 is solved iteratively until the residual terms on the right side vanish at the configuration time t_n. To solve Eq. 14, the kinematic relation in Eq. 15 is substituted into the structural bilinear form $a^*({}^n z^k;\Delta z^{k+1},\bar{z})$ to express the unknown Δz^{k+1} in terms of $\Delta z^{k+1}_{,tt}$ as

$$d(\Delta z^{k+1}_{,tt},\bar{z}) + \beta \Delta t^2 a^*({}^n z^k;\Delta z^{k+1}_{,tt},\bar{z}) = \ell(\bar{z}) - a({}^n z^k,\bar{z}) - d({}^n z^k_{,tt},\bar{z}), \quad \forall \bar{z} \in Z \tag{17}$$

which is solved for the incremental acceleration $\Delta z^{k+1}_{,tt}$.

After computing $\Delta z^{k+1}_{,tt}$, the displacement and velocity are updated using Eqs. 9 and 16. The tangent stiffness matrix obtained from Eq. 17 is stored for the DSA described in the following section. The path-dependent terms, including internal plastic variables (back stress and effective plastic strain), are updated in the same way as the classical infinitesimal elastoplasticity [15]. In addition, the stress-free intermediate configuration $\boldsymbol{F}^p$ is updated using the following incremental plastic deformation gradient as

$$\boldsymbol{f}^p = \sum_{j=1}^{3} \exp(-\xi N_j) \boldsymbol{n}^j \otimes \boldsymbol{n}^j \tag{18}$$

where $\boldsymbol{n}^j$ is the principal vector of Kirchhoff stress, ξ is the plastic consistency parameter determined by the return-mapping algorithm, and $\boldsymbol{N}$ is the unit normal vector of von Mises yield surface in the principal stress space. Note that $\boldsymbol{f}^p$ is a

symmetric tensor, which implies that the incremental plastic spin vanishes. Thus, the following updated formulas can be used:

$$\boldsymbol{F}_n^e = \boldsymbol{f}^p \boldsymbol{F}_n^{e^{tr}} \tag{19}$$

$$\boldsymbol{F}_n^p = \boldsymbol{F}_n^{e^{-1}} \boldsymbol{F}_n \tag{20}$$

where the superscript *tr* denotes the elastic trial states by assuming all the incremental deformation is elastic. This formulation is different from that of Simo [14], for which all the rigid body rotations are ignored in $\boldsymbol{F}^e$, and only $\boldsymbol{b}^e = \boldsymbol{F}^e \boldsymbol{F}^{eT}$ is stored from the isotropic assumption. From an analysis viewpoint, this is possible since the rigid body motion does not contribute to the constitutive relation. However, for shape DSA, a discontinuous intermediate configuration is not allowed since continuous perturbation of the domain is considered. Thus, the decomposition in Eqs. 18–20 has to be used to recover the finite elasticity when no plastic flow is observed. However, more memory is required to store nonsymmetric $\boldsymbol{F}^p$ rather than the symmetric $\boldsymbol{b}^e$.

III. SHAPE DESIGN SENSITIVITY ANALYSIS OF DYNAMICS

In shape DSA, the structural domain shape is the design. Let initial domain ${}^0\Omega(\boldsymbol{X})$ be perturbed in the direction of $\boldsymbol{V}(\boldsymbol{X})$ (design velocity), and the magnitude of the perturbation is controlled by a scalar parameter τ to the new domain ${}^0\Omega_\tau(\boldsymbol{X}_\tau)$. Shape DSA is used to obtain the variation of the state variable in terms of the design velocity explicitly using the direct differentiation method. The material derivative concept in continuum mechanics is utilized to describe the design variation. The material derivative of the displacement can be expressed as a sum of the partial derivative and convective terms as

$$\begin{aligned} \dot{\boldsymbol{z}} &= \lim_{\tau \to 0} \frac{1}{\tau} \boldsymbol{z}_\tau(\boldsymbol{X} + \tau \boldsymbol{V}) - \boldsymbol{z}(\boldsymbol{X})] \\ &= \boldsymbol{z}' + \nabla\, {}^0\boldsymbol{z} \boldsymbol{V} \end{aligned} \tag{21}$$

where $\nabla_0 \boldsymbol{z} = [\partial z_i / \partial X_j]$ is the gradient of $\boldsymbol{z}$ with respect to the undeformed configuration.

For the linear problem, it has been shown that the displacement $\boldsymbol{z}$ is Fréchet differentiable with respect to the design [16]. Without mathematical support, it is assumed that the displacement $\boldsymbol{z}$ is differentiable formally for the nonlinear structural dynamic problem. Assume that response analysis is converged up to time t_n, and the sensitivity equation is solved up to time t_{n-1}. The design sensitivity equation at time t_n can be obtained by taking the material derivative of Eq. 1 as

$$\frac{d}{d\tau}[d({}^{n}z_{,it},\bar{z})] + \frac{d}{d\tau}[a({}^{n}z,\bar{z})] = \frac{d}{d\tau}[\ell(\bar{z})], \qquad \nabla\bar{z} \in Z \tag{22}$$

The material derivative formulas of the structural energy and load forms are discussed in detail in the work of Kim et al. [8]. If the hyperelasticity-based constitutive relation is used, then the sensitivity equation is solved for the material derivative of the total displacement. Since the design perturbation occurs at the initial configuration ($t = 0$), the structural variational form $a(z,\bar{z})$ is transformed to the initial configuration (pull back) and then transformed to the current configuration (push forward) after taking the derivative with respect to the design. The material derivative of the structural energy form, using the updated Lagrangian formulation, becomes

$$\frac{d}{d\tau}[a(z,\bar{z})] = a^{*}(z;\dot{z},\bar{z}) + a'_{V}(z,\bar{z}) \tag{23}$$

where $a^{*}(z;\dot{z}\bar{z})$ is the same form as the structural bilinear form in Eq. 13 if Δz is substituted by $\dot{z}$ and

$$a'_{V}(z,\bar{z}) = \int_{0_\Omega} (\bar{\varepsilon}_{ij} c_{ijkl} \varepsilon^{V}_{kl}(z) + \bar{\varepsilon}_{ij} c_{ijkl} \varepsilon^{P}_{kl}(z) + \tau^{fic}_{ij} \bar{\varepsilon}_{ij}) d\Omega + \int_{0_\Omega} (\tau_{ij} \eta^{ij}_{V}(z,\bar{z}) + \tau_{ij} \eta^{P}_{ij}(z,\bar{z}) + \tau_{ij} \bar{\varepsilon}_{ij} div\boldsymbol{V}) d\Omega \tag{24}$$

is the structural fictitious load form. The form $a'_{V}(z,\bar{z})$ depends explicitly on the design perturbation through the design velocity $\boldsymbol{V}(\boldsymbol{X})$, the structural response z, and the material derivatives of path-dependent variables. In Eq. 24,

$$\boldsymbol{\varepsilon}^{V}(z) = -sym\ (\nabla_{0} z \nabla_{n} \boldsymbol{V}) \tag{25}$$

$$\boldsymbol{\eta}^{V}(z,\bar{z}) = -sym(\nabla_{n} \bar{z}^{T} \nabla_{0} z \nabla_{n} \boldsymbol{V}) - sym(\nabla_{0} \bar{z} \nabla_{n} \boldsymbol{V}) \tag{26}$$

explicitly depend on design velocity $\boldsymbol{V}(\boldsymbol{X})$ and z, and

$$\boldsymbol{\varepsilon}^{p}(z) = -sym(\boldsymbol{G}) \tag{27}$$

$$\boldsymbol{\eta}^{p}(z,\bar{z}) = -sym(\nabla_{n} \bar{z} \boldsymbol{G} + \nabla_{n} \bar{z}^{T} \boldsymbol{G}) \tag{28}$$

$$\boldsymbol{G} = \boldsymbol{F}^{e} \frac{d}{d\tau}(\boldsymbol{F}^{p}) \boldsymbol{F}^{-1} \tag{29}$$

depend on the material derivative of the intermediate configuration, and τ^{fic} represents the sensitivity of path-dependent plastic variables. Notations $\nabla_0 \bar{z} = \partial \bar{z}/\partial \boldsymbol{X}$, $\nabla_n \bar{z} = \partial \bar{z}/\partial \boldsymbol{x}$, and $sym(\boldsymbol{A}) = \frac{1}{2}(\boldsymbol{A} + \boldsymbol{A}^{T})$ are used throughout this paper. Equation 29 corresponds to transforming (push forward) the material derivative of $\boldsymbol{F}^{p}$ into the current configuration for the updated Lagrangian description.

For the case of a conservative external load, the design variation of the load form contains explicitly dependent terms only:

$$\frac{d}{d\tau}[\ell(\bar{z})] = \ell'_V(\bar{z}) \tag{30}$$

where

$$\ell'_V(\bar{z}) = \int_{0_\Omega} (\bar{z}^T(\nabla \boldsymbol{f}^{\,b}\boldsymbol{V}) + \bar{z}^T \boldsymbol{f}^{\,b} div\boldsymbol{V}) d\Omega + \int_{0_{\Gamma^h}} (\bar{z}^T(\nabla \boldsymbol{f}^{\,h}\boldsymbol{V}) + \kappa \bar{z}^T \boldsymbol{f}^{\,h} V_n) d\Gamma \tag{31}$$

κ is the curvature of the boundary, and V_n is the normal component of the design velocity on the boundary. In Eqs. 24 and 31, $a'_V(z,\bar{z})$ and $\ell'_V(\bar{z})$ can be computed using the results of response analysis up to time t_n and sensitivity analysis up to time t_{n-1} with a given design velocity field at the undeformed configuration.

The design sensitivity of the kinetic energy form is relatively simple compared to that of the structural energy form using the principle of mass conservation, for which integration is carried out at the undeformed configuration. The material derivative of the kinetic energy form is

$$\frac{d}{d\tau}[d(z_{,tt},\bar{z})] = \int_{0_\Omega} \rho \bar{z}^T \dot{z}_{,tt}\, d\Omega + \int_{0_\Omega} \rho \bar{z}^T z_{,tt} div\boldsymbol{V}\, d\Omega \equiv d(\dot{z}_{,tt},\bar{z}) + d'_V(z_{,tt},\bar{z}) \tag{32}$$

where $d'_V(z_{,tt},\bar{z})$ contains the divergence term only. Relatively simple expression is obtained for kinetic energy form in Eq. 32 since no spatial derivative of state variable is involved.

Using Eqs. 23, 30, and 32, the design sensitivity Eq. 22 for structural transient dynamics can be expressed as

$$d({}^n\dot{z}_{,tt},\bar{z}) + a^*({}^n z; {}^n\dot{z},\bar{z}) = \ell'_V(\bar{z}) - a'_V({}^n z,\bar{z}) - d'_V({}^n z_{,tt},\bar{z}), \qquad \forall \bar{z} \in Z \tag{33}$$

The design sensitivity Eq. 33 is another IBVP, which requires the initial conditions. Since the initial conditions in Eqs. 7 and 8 are fixed values, their material derivatives vanish. Thus, the initial conditions for the sensitivity equation become

$$\dot{z}(\boldsymbol{X},0) = \boldsymbol{0} \qquad \boldsymbol{X} \in {}^0\Omega \tag{34}$$

$$\dot{z}_{,t}(\boldsymbol{X},0) = \boldsymbol{0} \qquad \boldsymbol{X} \in {}^0\Omega \tag{35}$$

and the time integration of the material derivatives of the kinematic variables follow the same procedure as response analysis:

$${}^n\dot{z}_{,t} = {}^n\dot{z}^{pr}_{,t} + \gamma\Delta t\, {}^n\dot{z}_{,tt} \tag{36}$$

$${}^n\dot{z} = {}^n\dot{z}^{pr} + \beta\Delta t^2\, {}^n\dot{z}_{,tt} \tag{37}$$

where material derivatives of predictors can be obtained from results at the previous time by

$$ {}^{n}\dot{z}_{,t}^{pr} = {}^{n-1}\dot{z}_{,t} + (1-\gamma)\Delta t\ {}^{n-1}\dot{z}_{,tt} \tag{38} $$

$$ {}^{n}\dot{z}^{pr} = {}^{n-1}\dot{z} + \Delta t\ {}^{n-1}\dot{z}_{,t} + (\tfrac{1}{2}-\beta)\Delta t^{2}\ {}^{n-1}\dot{z}_{,tt} \tag{39} $$

with Eqs. 34 and 35 as initial conditions. By using Eq. 37, Eq. 33 is expressed in terms of the acceleration sensitivity as

$$ d({}^{n}\dot{z}_{,tt},\bar{z}) + \beta\Delta t^{2} a^{*}({}^{n}z;\ {}^{n}\dot{z}_{,tt},\bar{z}) = \ell'_{V}(\bar{z}) - a'_{V}({}^{n}z,\bar{z}) - d'_{V}({}^{n}z_{,tt},\bar{z}) - a^{*}({}^{n}z;\ {}^{n}\dot{z}^{pr},\bar{z}), \quad \forall \bar{z} \in Z \tag{40} $$

The left side of Eq. 40 has the same form as response analysis in Eq. 17 with a different right side, which is the fictitious load. The sensitivity equation solves the number of design parameters at a given time. Thus, the decomposition of the matrix is important for efficiency. Note that the sensitivity Eq. 40 does not require any convergence iteration, whereas response analysis is solved iteratively to obtain the converged configuration in Eq. 14. Thus, a linear sensitivity equation is solved at each converged time step effectively. Note that the last term in Eq. 40 $a^{*}({}^{n}z;{}^{n}\dot{z}^{pr},\bar{z})$ is the contribution from the time integration effect of structural dynamics, which does not appear in a quasi-static sensitivity equation.

An interesting observation comes from the comparison of the sensitivity equation with that of the quasi-static problem for elastic material. It is well known that the sensitivity equation is solved only once at the final converged time for the quasi-static problem. However, the sensitivity Eq. 40 is solved at each converged time step for the dynamic problem regardless of the constitutive model.

After solving for the acceleration sensitivity in Eq. 40, the velocity and displacement sensitivities are obtained using Eqs. 36 and 37. The material derivatives of the internal plastic variables are also updated for the sensitivity computation at the next time. This procedure is the same as the infinitesimal elastoplasticity formulation in the principal stress space [15].

The last part of DSA is updating the material derivative of the intermediate configuration $\boldsymbol{F}^{p}$. For a given $\dot{z}$, the material derivative of the deformation gradient can be computed using

$$ \frac{d}{d\tau}(\boldsymbol{F}) = \frac{d}{d\tau}(\boldsymbol{I} + \nabla_{0}z) = \nabla_{0}\dot{z} - \nabla_{0}z\nabla_{0}V \tag{41} $$

with the analysis result z and design velocity $\boldsymbol{V}$. By taking the material derivative of the multiplicative decomposition in Eq. 20, the material derivative of $\boldsymbol{F}^{p}$ can be obtained as

$$ \frac{d}{d\tau}(\boldsymbol{F}_{n}^{p}) = \frac{d}{d\tau}(\boldsymbol{F}_{n}^{e^{-1}})\boldsymbol{F}_{n} + \boldsymbol{F}_{n}^{e^{-1}}\frac{d}{d\tau}(\boldsymbol{F}_{n}) \tag{42} $$

where the material derivative of $\boldsymbol{F}^{e}$ can be obtained from Eq. 19 as

$$\frac{d}{d\tau}(\boldsymbol{F}_n^e) = \frac{d}{d\tau}(\boldsymbol{f}^p)\boldsymbol{F}_n^{e^{tr}} + \boldsymbol{f}^p \frac{d}{d\tau}(\boldsymbol{F}_n^{e^{tr}}) \tag{43}$$

and its inverse from the relation $\frac{\mathrm{d}}{\mathrm{d}\tau}(\boldsymbol{F}_n^e \boldsymbol{F}_n^{e^{-1}}) = 0$, as

$$\frac{d}{d\tau}(\boldsymbol{F}_n^{e^{-1}}) = -\boldsymbol{F}_n^{e^{-1}} \frac{d}{d\tau}(\boldsymbol{F}_n^e)\boldsymbol{F}_n^{e^{-1}} \tag{44}$$

IV. REVIEW OF THE MESH-FREE METHOD

The theory of the mesh-free method was developed recently to remove or reduce the mesh dependence of the conventional finite-element method. Few references concerning the mesh-free method can be found in literature [13, 17–23]. The shape function is not a function of the reference domain, but a function of the material points, and the order of shape function can be changed easily. Insensitivity to the mesh distortion is a very important feature in nonlinear analysis and shape optimization. Higher accuracy can be achieved by simply adding more nodes to the structure without remodeling the total structure. However, the difficulty in imposing the essential boundary condition and relatively high cost of analysis are weaknesses in spite of the aforementioned advantages. The mesh-free method is chosen as an analysis tool for this paper.

Consider an approximation of a scalar displacement $z(x)$ using an integral transformation with a kernel function $\phi_a(y - x)$ as

$$z^S(x) = \int_{-\infty}^{\infty} \phi_a(y - x)z(y)dy \tag{45}$$

If the kernel function $\phi_a(y - x)$ has the Dirac delta property, the kernel estimate $z^S(x)$ exactly represents displacement $z(x)$. However, the approximation in Eq. 45 in the finite domain shows errors around boundary and amplitude and phase errors in the domain.

Liu et al. [20] developed the reproducing kernel particle method (RKPM) by introducing a modified kernel function that is constructed based on the enforcement of reproducing conditions such that the kernel estimate of displacement exactly reproduces polynomials. In RKPM, a displacement function $z(x)$ is approximated using a modified kernel estimate

$$z^R(x) = \int_\Omega \tilde{\phi}_a(s - y)z(y)dy \tag{46}$$

where $z^R(x)$ is the reproduced displacement function of $z(x)$ and $\tilde{\phi}_a(s - x)$ is the modified kernel function with a support measure of a to satisfy the completeness condition.

To develop a shape function for discrete approximation, Eq. 46 is discretized. Suppose that the domain ${}^0\Omega$ is discretized by a set of nodes $[x_1, \ldots x_I, \ldots, x_{NP}]$, where x_I is the location of node I, and NP is the total number of nodes. Using a simple trapezoidal rule, Eq. 46 is discretized into

$$z^R(x) = \sum_{I=1}^{NP} \Phi_I(\boldsymbol{x}) d_I \tag{47}$$

where $\Phi_I(x)$ is interpreted as the mesh-free shape function of node I, and d_I is the associated coefficient of approximation, often called the *generalized displacement*. The shape function $\Phi_I(x_J)$ depends on the current coordinate x_J, whereas the shape function of the finite-element method depends only on a coordinate of reference geometry. It should also be noted that, in general, the shape function does not bear the Kronecker delta properties, that is, $\Phi_I(x_J) \neq \delta_{IJ}$. Therefore, for a general function $z(x)$ that is not a polynomial, d_I in Eq. 47 is not the nodal value of $z(x)$. The domain is discretized by nonoverlapping regions (integration zone), and standard Gauss integration is used to evaluate the domain integral (Fig. 1). This domain partitioning is independent of the nodal locations, and nodes are not interconnected by elements. The response variables (for example, displacements) are defined at the nodes independent of the integration zones.

V. DESIGN OPTIMIZATION

A vehicle bumper is installed to protect the body from impact and to absorb the impact energy through the plastic deformation. Vehicle design regu-

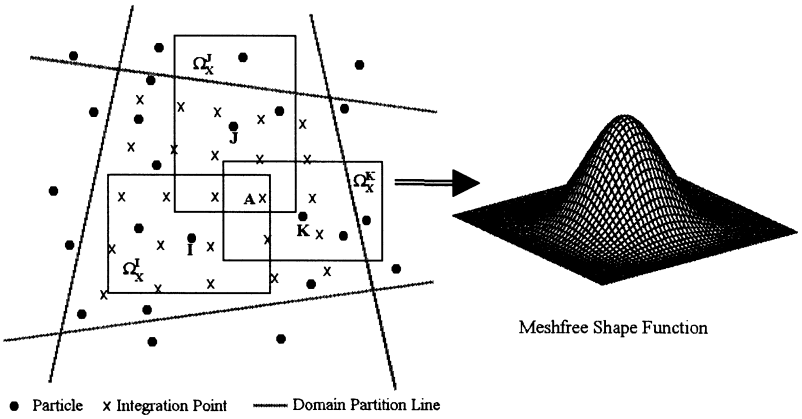

Figure 1. Domain discretization and mesh-free shape function.

lations require that the bumper be safe up to a 5 mph impact. In this section, design optimization of a vehicle bumper structure is performed to reduce the plastic deformation. The design optimization problem based on a quasi-static assumption was presented by Kim et al. [8]. However, an actual impact happens in a very short time period even in a 5 mph impact situation. The same problem is solved with a transient dynamic assumption in this article.

The cross section of the metal bumper is approximated using 144 mesh-free particles and 71 integration zones (Fig. 2). The upper and lower parts of the bumper are attached to the vehicle. The elastoplastic material constants are Young's modulus $E = 206.9$ GPa, the Poisson ratio $\nu = 0.29$, plastic hardening modulus $H = 1.1$ GPa, and initial yield stress $\sigma_y = 0.5$ GPa. Linear isotropic hardening is considered when the plastic consistency condition can be solved explicitly without iteration. The Newmark implicit time integration method is used with parameters $\beta = 0.26$ and $\gamma = 0.5$ and the density $\rho = 7800$ kg/m^3. Response analysis is carried out up to 0.01 s. Since the problem includes impact with a rigid surface, the following linear system of the equation is solved instead of Eq. 17:

$$d(\Delta z^{k+1}_{,tt}, \bar{z}) + \beta \Delta t^2 [a^*(z^k; \Delta z^{k+1}_{,tt}, \bar{z}) + b^*(z^k; \Delta z^{k+1}_{,tt}, \bar{z})] = \ell(\bar{z}) - a(z^k, \bar{z}) - b(z^k, \bar{z}) - d(z^k_{,tt}, \bar{z}), \qquad \forall \bar{z} \in Z \tag{48}$$

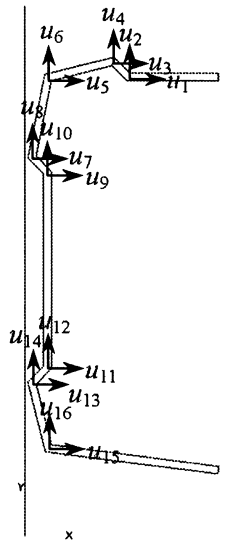

Figure 2. Bumper cross-section geometry and shape design parameterization.

where $b(z,\bar{z})$ and $b^*(z;\Delta z,\bar{z})$ are the frictional contact variational form and its linearization, respectively. Figure 3 shows the contour plots of the effective plastic strain and von Mises stress at the final time, respectively. The vertical coordinate of the lower contact point remains almost constant for the quasi-static case because of frictional effects, whereas in the transient dynamic case, the contact point moves up since no friction is applied during the oscillating period between a contact and noncontact situation. Most of the contact forces are retained by two end points. The concentration of the plastic strain appears at the upper part of the bumper, and the stress concentration magnitude is similar at the upper and lower parts. Figure 4 shows the time history of the displacement, velocity, and acceleration of the upper contact point. A very high frequency response is observed for acceleration.

The boundary of the bumper is represented by a cubic spline curve, and

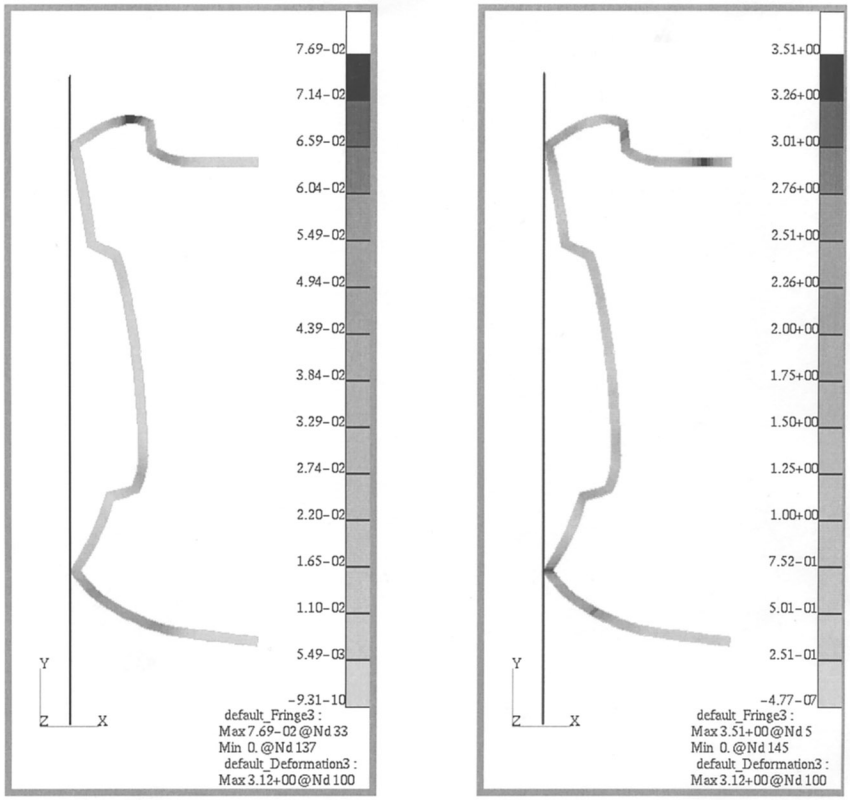

Figure 3. Plastic strain and von Mises stress distributions.

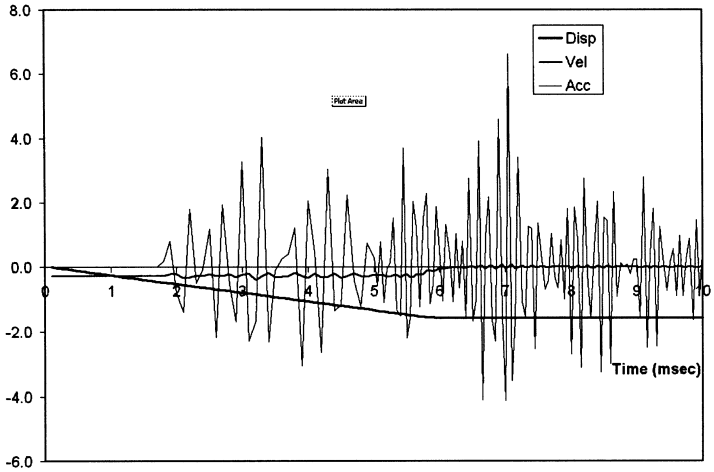

Figure 4. Time history of displacement, velocity, and acceleration.

each particle point on the boundary has a unique parametric representation. The locations of the control points of each boundary curve are the shape design parameters. The design velocity vector corresponding to the particle point can be computed using parametric representation. Since the bumper is usually manufactured by a sheet metal stamping process, it is inappropriate to change the thickness at each section. To maintain the constant thickness of 0.5 cm, design parameters are linked in the thickness directions corresponding to the inner/outer control points. The 16 shape design parameters are chosen as shown in Fig. 2. After choosing the design parameters, the design velocity field is obtained by perturbing the boundary curve in the direction of each design parameter.

Using the design velocity information, DSA is carried out. Since the problem includes impact with a rigid surface, the following linear system of the sensitivity equation is solved instead of Eq. 40:

$$d(\dot{z}_{,tt},\bar{z}) + \beta\Delta t^2[a^*(z;\dot{z}_{,tt},\bar{z}) + b^*(z;\dot{z}_{,tt},\bar{z})] = \ell'_V(\bar{z}) - a'_V(z,\bar{z}) - b'_V(z,\bar{z}) - d'_V(z_{,tt},\bar{z}) - a^*(z;\dot{z}^{pr},\bar{z}) - b^*(z;\dot{z}^{pr},\bar{z}), \qquad \forall \bar{z} \in Z \tag{49}$$

where $b'_V(z,\bar{z})$ is the contact fictitious load derived by Kim et al. [12]. The linear system of Eq. 49 is solved using the factorized tangent stiffness matrix from response analysis with the fictitious load. No iteration is required to solve the sensitivity equation, but Eq. 49 is solved for the number of design parameters. This procedure is quite efficient compared to iterative response analysis. The sensitivity coefficients of the performance measures are computed after solving

the design sensitivity equation at the final converged load step. Possible performance measures are the displacement, stress tensor, internal plastic variables, reaction force, contact force, and normal gap distance.

To show the efficiency of the proposed method, the computation times of response analysis and DSA are compared. The response analysis requires 1599 s, whereas DSA requires 853 s for 16 design parameters, which is less then 3.3% of the response analysis time per design parameter. This ratio is quite efficient compared to the finite difference method. This efficiency is because the sensitivity equation is solved without iteration, and the factorized tangent stiffness matrix from response analysis is used. Table 1 shows the sensitivity coefficients and comparison of sensitivity results with the finite difference results. Very accurate sensitivity results are obtained even for the highly nonlinear behavior of the problem. In Table 1, the second column $\Delta\Psi$ denotes the first-

Table 1. Comparison of Sensitivity Results

Design	ψ	$\Delta\psi$	ψ'	$(\Delta\psi/\psi') \times 100$
u_2	e^p_{15}	–0.754098E – 7	–0.754105E – 7	100.00
	e^p_{65}	0.313715E – 7	0.313668E – 7	100.02
	e^p_{29}	0.441192E – 7	0.441162E – 7	100.01
	z_{x39}	0.790973E – 5	0.791092E – 5	99.98
	F_{Cx100}	–0.657499E – 6	–0.657074E – 6	100.06
u_4	e^p_{15}	0.268699E – 6	0.268712E – 6	100.00
	e^p_{65}	–0.843101E – 9	–0.863924E – 9	97.59
	e^p_{29}	0.123988E – 6	0.123993E – 6	100.00
	z_{x39}	–0.847749E – 5	–0.847586E – 5	100.02
	F_{Cx100}	0.410724E – 7	0.407515E – 7	100.79
u_6	e^p_{15}	–0.317362E – 6	–0.317349E – 6	100.00
	e^p_{65}	–0.640031E – 7	–0.640159E – 7	99.98
	e^p_{29}	–0.163051E – 6	–0.163051E – 6	100.00
	z_{x39}	–0.190521E – 5	–0.190392E – 5	100.07
	F_{Cx100}	0.473040E – 6	0.472876E – 6	100.03
u_8	e^p_{15}	0.888094E – 8	0.890589E – 8	99.72
	e^p_{65}	0.355128E – 7	0.354794E – 7	100.09
	e^p_{29}	–0.981276E – 8	–0.981572E – 8	99.97
	z_{x39}	–0.239706E – 5	–0.239333E – 5	100.16
	F_{Cx100}	–0.184457E – 6	–0.183954E – 6	100.27
u_{10}	e^p_{15}	–0.642594E – 8	–0.643542E – 8	99.85
	e^p_{65}	–0.151580E – 7	–0.151527E – 7	100.03
	e^p_{29}	0.172663E – 7	0.172698E – 7	99.98
	z_{x39}	–0.154011E – 5	–0.154125E – 5	99.93
	F_{Cx100}	–0.134372E – 6	–0.134701E – 6	99.76

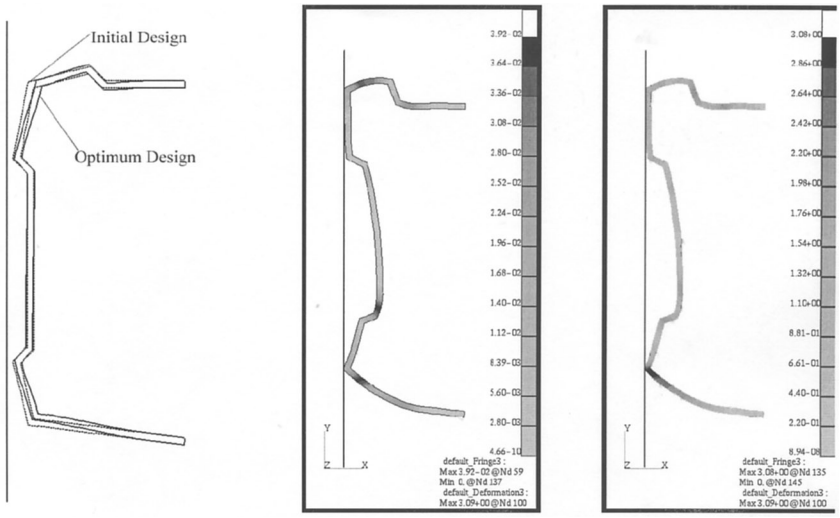

(a) (b) (c)

Figure 5. Analysis results at optimum design: (a) optimum geometry; (b) plastic strain; (c) von Mises stress.

order sensitivity results from the forward finite difference method using a perturbation of $\tau = 10^{-6}$, and the third column represents the sensitivity computation results of the proposed method. In the first column, z, e^p, and F_C are such performance measures as the displacement, effective plastic strain, and contact force, respectively. For example, e^p_{15} denotes the effective plastic strain at integration zone 15, and F_{Cx100} denotes the x-directional contact forces at the slave node 100.

Since the bumper is mass-produced, any small reduction in weight can provide significant cost savings. The safety of the bumper, however, is an important criterion to the performance. Thus, a design optimization problem can be formulated such that the area of the bumper cross section is minimized with reduced effective plastic strains and the same contact force as the initial design.

Table 2. Structural Performance Measures

Type	Initial Design	Optimum Design
$e^p_{\max}$	0.0769	0.0392
Area	24.27	23.90
F_C	2.009	2.056

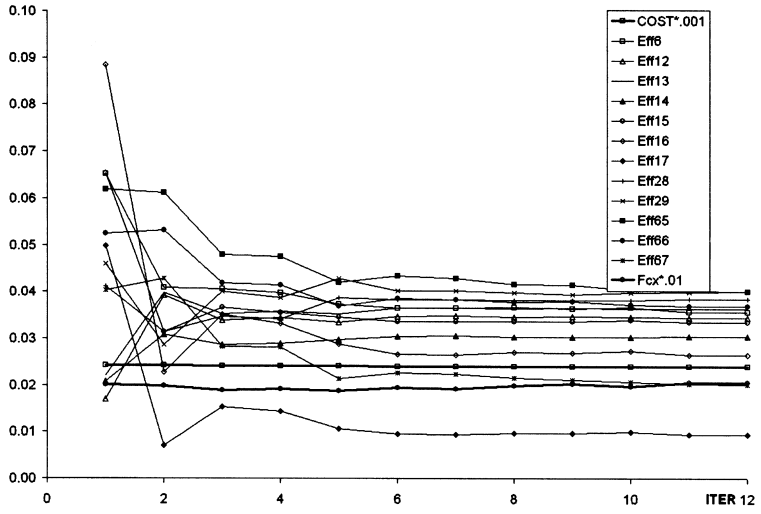

Figure 6. Design optimization history.

The following equation shows a design optimization problem with 15 constraints for the effective plastic strains and 1 for the normal contact force in the x direction:

$$\begin{aligned} &\text{Minimize} && Area \\ &\text{Subject to} && e^{p}_{\max} \le 0.04 \\ &&& \boldsymbol{F}_{Cx}(2.0) \ge 2.0 \\ &&& -1.0 \le u_j \le 1.0 \end{aligned} \tag{50}$$

The design optimization is carried out using the sequential quadratic programming method in DOT [24]. The performance values are provided to DOT from nonlinear mesh-free analysis, and the sensitivity coefficients are provided using the proposed method. The optimization problem is converged after 12 iterations, and all the constraints are satisfied. Figure 5 shows the optimized design and the response analysis results. In the optimum design, u_5 and u_{15} are increased, yielding larger approach angles for both upper and lower parts such that, after impact, the point contacts of the initial design (Fig. 3) are changed to a line contact as shown in Fig. 5b. Table 2 compares the maximum of the effective plastic strain and contact force of the initial and optimum designs. Most of the design iteration is used to correct constraint violations in the effective plastic strains while maintaining the contact force.

Figure 6 shows the design history of the cost function and constraints.

After iteration number 5, no significant changes in cost and constraints are observed. However, design parameters continue to change during these iterations to find the optimum design. At the optimum design, six constraints for the effective plastic strains and the normal contact force are active.

VI. CONCLUSION

An accurate and efficient shape DSA and optimization of structural transient dynamics are proposed for finite deformation elastoplastic materials, including impact with a rigid surface. It is shown that the design sensitivity equation is solved at each converged time step using the same tangent stiffness matrix as response analysis without iteration. It is noted that the sensitivity equation is more efficient for the implicit time integration method than for the explicit method compared to the cost of response analysis.

ACKNOWLEDGMENT

This research was supported by NSF/DARPA Optimized Portable Algorithms and Applications Libraries (OPAAL) (contract 9874015).

REFERENCES

1. Belytschko, T. A Survey of Numerical Methods and Computer Programs for Dynamic Structural Analysis. Nuclear Eng. Design **1976**, *37*, 23–34.
2. Hilber, H.M.; Hughes, T.J.R. Colocation, Dissipation, and Overshoot for Time Integration Schemes in Structural Dynamics. Earthquake Eng. Struct. Dyn. **1978**, *6*, 99–117.
3. Tortorelli, D.A.; Lu, S.C.Y.; Haber, R.B. Adjoint Sensitivity Analysis for Nonlinear Dynamic Thermoelastic Systems. AIAA J. **1991**, *29*, 253–263.
4. Poldneff, M.J.; Arora, J.S. Design Sensitivity Analysis in Dynamic Thermo-Viscoelasticity with Implicit Integration. Int. J. Solids Struct. **1996**, *33*, 577–594.
5. Pollock, G.D.; Noor, A.K. Sensitivity Analysis of the Contact/Impact Response of Composite Structures. Comp. Struct. **1996**, *61*, 251–269.
6. Arora, J.S.; Dutta A. Explicit and Implicit Methods for Design Sensitivity Analysis of Nonlinear Structures Under Dynamic Loads. Appl. Mech. Rev. **1997**, *50*, 11–19.
7. Choi, K.K.; Cho S. Design Sensitivity Analysis and Optimization of Nonlinear Structural Dynamics Using DYNA3D. In *Seventh AIAA/USAF/*

NASA/ISSMO Symposium on Multidisciplinary Analysis and Optimization, St. Louis, MO, September 2–4, 1998; American Institute of Aeronautics and Astronautics: Washington, DC, 1998; 1071–1081.
8. Kim, N.H.; Choi, K.K.; Chen, J.S. Shape Design Sensitivity Formulation for Finite Deformation Elastoplasticity with Contact. In *Third World Congress of Structural and Multidisciplinary Optimization*; May 17–21, Buffalo, NY, 1999; International Society of Structural and Multidisciplinary Optimization; 662–664.
9. Haug, E.J.; Choi, K.K.; Komkov, V. *Design Sensitivity Analysis of Structural Systems*; Academic Press: New York, 1986.
10. Hughes, T.J.R. *The Finite Element Method*; Prentice-Hall: Englewood Cliffs, NJ, 1987.
11. Bathe, K.J. *Finite Element Procedures*; Prentice Hall, Englewood Cliffs, NJ, 1996.
12. Kim, N.H.; Choi, K.K.; Chen, J.S.; Park, Y.H. Meshless Shape Design Sensitivity Analysis and Optimization for Contact Problem with Friction. Comp. Mech. **2000**, *25*, 157–168.
13. Chen, J.S.; Pan, C.; Wu, C.T.; Liu, W.K. Reproducing Kernel Particle Methods for Large Deformation Analysis of Nonlinear Structures. Comput. Methods Appl. Mech. Eng. **1996**, *139*, 195–227.
14. Simo, J.C. Algorithms for Static and Dynamic Multiplicative Plasticity That Preserve the Classical Return Mapping Schemes of the Infinitesimal Theory. Comput. Meth. Appl. Mech. Eng. **1992**, *99*, 61–112.
15. Kim, N.H; Choi, K.K.; Chen, J.S. Shape Design Sensitivity Analysis and Optimization of Elastoplasticity with Frictional Contact. AIAA J. **2000**, *38*, 1742–1753.
16. Rousselet, B. Quelques Resultats en Optimisation de Domains; thesis; University of Nice, 1982.
17. Lancaster, P.; Salkauskas K. Surface Generated by Moving Least Squares Methods. Math. Comp. **1981**, *37*, 141–158.
18. Nayroles, B.; Touzot, G.; Villon, P. Generalizing the Finite Element Method: Diffuse Approximation and Diffuse Elements. Comp. Mech. **1992**, *10*, 307–318.
19. Belytschko, T.; Lu, Y.Y.; Gu, L. Element Free Galerkin Method. Int. J. Num. Meth. Eng. **1994**, *37*, 229–256.
20. Liu, W.K.; Jun, S.; Zhang, Y.F. Reproducing Kernel Particle Methods. Int. J. Num. Meth. Fluids **1995**, *20*, 1081–1106.
21. Randles, P.W.; Libersky, L.D. Smoothed Particle Hydrodynamics: Some Recent Improvements and Applications. Comput. Meth. Appl. Mech. Eng. **1996**, *139*, 375–408.
22. Duarte, C.A.M.; Oden, J.T. A H-P Adaptive Method Using Clouds. Comput. Meth. Appl. Mech. Eng. **1996**, *139*, 237–262.

23. Melenk, J.M.; Babuska, I. The Partition of Unity Finite Element Method: Basic Theory and Applications. Comput. Meth. Appl. Mech. Eng. **1996**, *139*, 289–314.
24. Vanderplaats, G.N. *DOT User's Manual*; VMA Corp.: Colorado Springs, CO, 1997.

Received September 2000
Revised February 2001